Structures of bare and singly hydrated [M(Ura-H)(Ura)]+ (M = Mg, Ca, Sr, Ba) complexes in the gas phase by IRMPD spectroscopy in the fingerprint region

Barry Power, Violette Haldys, Jean-Yves Salpin, Travis D Fridgen

Structures of bare and singly hydrated $[M(Ura-H)(Ura)]^+$ (M=Mg, Ca, Sr, Ba) complexes in the gas phase by IRMPD spectroscopy in the fingerprint region.

Barry Power,[a] Violette Haldys,[b,c] Jean-Yves Salpin,[b,c*] and Travis D. Fridgen[a*]

a: Department of Chemistry, Memorial University, St. John's, NL, A1N 4T8, Canada.

b: Université d'Evry Val d'Essonne – Laboratoire d'Analyse et Modélisation pour la Biologie et l'Environnement – Bâtiment Maupertuis, Boulevard François Mitterrand, 91025 Evry, France

c: CNRS – UMR 8587

* jean-yves.salpin@univ-evry.fr, tfridgen@mun.ca

Abstract

The structures of deprotonated group 2 metal dication bound uracil dimers as well as the singly hydrated dimers were explored in the gas phase using infrared multiple photon dissociation (IRMPD) spectroscopy (1000–1900 cm^{-1}) in a Fourier transform ion cyclotron resonance mass spectrometer (FTICR-MS). The IRMPD spectra were then compared to computed IR spectra for various isomers. Calculations were performed using B3LYP with the 6-31+G(d,p) basis set for all atoms except Ba^{2+} and Sr^{2+}, for which the LANL2DZ or the def2-TZVPP basis sets with relativistic core potentials were used. The lowest energy structures are those in which the one uracil is deprotonated at the N3 position while the neutral uracil is a tautomer where the N3 hydrogen is at the O4 or O2 carbonyl oxygen and the metal is tetracoordinate interacting with N3 and O4 of deprotonated uracil and either N3 and O2 or N3 and O4 of neutral uracil. In the solvated complexes, the water molecule is also coordinated to the metal ion.

1. Introduction

Metal cations are known to play a central role in many biological systems. In particular, divalent cations have been shown to be crucial in the stability and activity of nucleic acids, as well as the folding of RNA structures [1–4]. These ions provide their stabilizing effect to the structure of DNA [5,6] and RNA [1], through both charge neutralization and noncovalent interactions with the phosphate backbone of the nucleic acids. Even in trace amounts, the interaction of metal cations with nucleic acids has a vital role in setting the course for the functionality of various biological molecules [7,8]; however, striking a balance is critical. Even though these metal ions play essential roles, the influence they hold over the behaviour of nucleic acids can often be detrimental. Unwanted conformational changes can result from an excess of metal dications, and through interaction of the ions with nucleobases themselves [2,6,9–13]. In particular, if nucleobases deviate from their canonical tautomer, improper base pairings and mutations are likely to result [14–17]. The interaction of metal ions with nucleobases has been the subject of many studies through a variety of techniques [18–32]. A major obstacle is the difficulty to replicate a cellular environment in condensed phase analysis. Rather, gas phase conditions are desired to allow for direct structural examination without the hindrance of bulk solvents, which may otherwise alter the complex structure. To accomplish this, action or consequence spectroscopy has been employed recently. In particular, infrared multiple photon dissociation (IRMPD) is a technique that has been successfully applied in many of these studies, and is the method of choice for this research.

The conventional numbering scheme for uracil is presented in Scheme 1. The most stable form of neutral uracil is the canonical, 2-4 diketo tautomer, in both the solid and gas phases [33–51]. However, metal ions have the ability to stabilize the keto-enol tautomer. Even

though alkaline earth dications do not have as strong an affinity towards nucleobases as transition metal dications [52], similar effects are observed. Trujillo and coworkers determined that in $[Ca(Ura)]^{2+}$, uracil tautomerizes to the 4-enol form, and the calcium ion bridges the O2 and dehydrogenated N3 atoms [53]. While such complexes having the form $[M(Ura)]^{2+}$ are stable in the case of alkaline-earth metals like Ca, the Pb^{2+} ion or transition dications such as Ni^{2+} and Cu^{2+}, will lead to deprotonation of the uracil moiety. For example, the lead(II)-uracil complex, $[Pb(Ura\text{-}H)]^{+}$, shows a preference towards the canonical, 2,4-diketo conformation of uracil [18] but it is deprotonated at N3. Although the monomeric complexes formed may differ based upon the interaction between the ion and uracil (electrostatic vs covalent), the dimeric complexes $[M(Ura\text{-}H)(Ura)]^{+}$ all behave similarly in the fact that one uracil is deprotonated, and the other remains neutral. The $[M(Ura)_2]^{2+}$ complex is generally not observed in the gas phase.

Previous works have determined that in these dimeric complexes the dication is tetracoordinate regardless of whether it is a transition metal [22,27] or alkaline earth metal [31]. The neutral uracil in the lowest energy complex is an enol, which participates in a hydrogen bond with a carbonyl of the neighbouring deprotonated uracil. Although good agreement was obtained between the computed lowest energy structures and the experimental spectra in each case, spectroscopically the exact placement of metal ion coordination could not be determined. In the N-H/O-H stretching region which was used to examine these complexes, no distinction could be made between those where the neutral uracil was the O2 or O4 enol resulting in the metal binding to N3 and O4 or N3 and O2, respectively. Even though the general structures of these dimeric complexes are expected to be similar for all dications, the pathway of fragmentation differs. Within the alkaline earth group, Ba^{2+} and Sr^{2+} complexes fragment by

loss of uracil, while Ca^{2+} and Mg^{2+} complexes lose an HNCO unit upon IRMPD or CID activation [30].

The current work aims to provide further insight into the previously examined [31] alkaline earth metal dimeric complexes, $[M(Ura-H)(Ura)]^+$, using IRMPD spectroscopy in the mid-infrared region, 1000–1900 cm^{-1}. In this fingerprint region, carbonyl stretching frequencies are obtained and distinguishing features between the N3O4 and N3O2 coordinated complexes are exposed. Along with the bare dimeric complexes, $[M(Ura-H)(Ura)]^+$, we also probe the singly hydrated complexes, $[M(Ura-H)(Ura)(H_2O)]^+$. The experimental spectra are compared to those computed using electronic structure calculations. A comparison of spectra and energies computed through different methods is also offered.

2. Methods

2.1. Experimental. All experiments were performed using a Fourier-transform ion cyclotron resonance mass spectrometer (FT-ICR-MS) coupled to a mid-infrared free electron laser (FEL) at the Centre Laser Infrarouge d'Orsay (CLIO) [54,55]. 0.01 M solutions of the chloride salts of each of the metal ions were prepared 18 MΩ water (Millipore). Uracil solutions were prepared to 1 mM in 18 MΩ water (Millipore). Mixtures were then prepared in a 1 to 10 ratio of metal solution to uracil solution, and introduced via syringe injection to the electrospray ion source at a flow rate of 75 μL/h. The ions were mass selected with a quadrupole mass filter and irradiated with the free electron laser following introduction and isolation into the ICR cell. Hydrated ions were prepared by first mass selecting the bare $[M(Ura)(Ura-H)]^+$ ion in the quadrupole filter and storing them in the hexapole storage cell into which water vapour had been leaked [56]. Irradiation times varied from 0.1 to 3 seconds, with the more weakly bound and, therefore, faster

dissociating hydrated ions being irradiated for the shortest time. Certain areas of the IRMPD spectra which were saturated were scanned after attenuation of the FEL. The laser was scanned at 5 cm^{-1} intervals from ~1000 to 1900 cm^{-1}. The IRMPD efficiency is the negative of the natural logarithm of parent ion intensity divided by the sum of parent and fragment ion signals.

2.2. Computational. Calculations for all structures were conducted using the Gaussian 09 suite of programs [57]. Each structure was optimized and infrared spectra computed using B3LYP density functional theory. In the cases of $[M(Ura\text{-}H)(Ura)]^+$ and $[M(Ura\text{-}H)(Ura)(H_2O)]^+$, where M = Ca^{2+} or Mg^{2+}, the 6-31+G(d,p) basis set was used for all atoms. For the $[M(Ura\text{-}H)(Ura)]^+$ and $[M(Ura\text{-}H)(Ura)(H_2O)]^+$ complexes, where M = Ba^{2+} and Sr^{2+}, the LANL2DZ basis set with relativistic core potential was used for strontium and barium atoms and the 6-31+G(d,p) basis was used for all other atoms. Single point energy calculations were then carried out using B3LYP with the 6-311+G(3df,3pd) basis set on all atoms except Sr and Ba for which the LANL2DZ basis set with relativistic core potential was used. This computational method will be referred to as method 1.

All calculations were then repeated, for the five lowest energy structures, with the def2-TZVPP basis set which has been found to work better for metal-cation amino acid complexes than the LANL2DZ [58,59] for all metals during both the optimization and single point energy calculations. The def2-TZVPP basis set contains polarization functions, which are not included in the LANL2DZ basis set. The 6-31+G(d,p) basis set was again used for all other atoms (C, H, N and O) during optimization, followed by the 6-311+G(3df,3pd) basis set for single point energy calculations. This computational method will be referred to as method 2.

These single-point electronic energies, using methods 1 and 2 were used to compute the enthalpies and Gibbs energies of isomeric species at 298K, using the unscaled harmonic vibrational frequencies calculated for optimization geometry.

The bonding within the individual equilibrium structures was also analyzed by locating the bond critical points (BCPs) using atoms-in-molecules (AIM) theory,[A] which is based on a topological analysis of the electronic density at the BCPs, and is a good descriptor of the bond strength or weakness. Data from the topological analysis are given in the Supporting Information.

[A] R. F. W. Bader, Atoms in molecules: a quantum theory, Clarendon Press ; Oxford University Press, Oxford, New York, 1990.

For comparison with the experimental spectra, the computed infrared spectra were all scaled by a factor of 0.97 and convoluted with a Lorentzian profile with a width (FWHM) of 15 cm^{-1}.

3. Results and Discussion

3.1. Examination of the IRMPD Spectra. When complexes were irradiated with the FEL, the following dissociation pathways were observed:

All M except Mg $[M(Ura\text{-}H)(Ura)]^+ \xrightarrow{IRMPD} [M(Ura\text{-}H)]^+ + Ura$

Following the loss of neutral Ura:

$M = Sr^{2+}$ $[M(Ura\text{-}H)]^+ \xrightarrow{IRMPD} [M(C_3H_2NO)]^+ + HNCO$

$M = Ca^{2+}, Mg^{2+}$ $[M(Ura\text{-}H)(Ura)]^+ \xrightarrow{IRMPD} [M(Ura\text{-}H)(C_2H_3)]^+ + HNCO + H_2CCO$

All M $[M(Ura\text{-}H)(Ura)(H_2O)]^+ \xrightarrow{IRMPD} [M(Ura\text{-}H)(Ura)]^+ + H_2O$

Following the loss of H_2O:

$M = Ca^{2+}$ $[M(Ura\text{-}H)(Ura)]^+ \xrightarrow{IRMPD} [M(Ura\text{-}H)(C_3H_3NO)]^+ + HNCO$

The observed dissociation pathways are in agreement with previous studies which determined the fragmentation for Ba^{2+} and Sr^{2+} uracil dimers occurs initially through loss of uracil, whereas Ca^{2+} and Mg^{2+} dimers undergo more complicated fragmentation beginning with the loss of HNCO [30].

Figure 1A shows the IRMPD spectra for $[M(Ura\text{-}H)(Ura)]^+$ in the 1000–1900 cm^{-1} region. All $[M(Ura\text{-}H)(Ura)]^+$ spectra display an intense band centred between 1614–1627 cm^{-1}, in the C=O stretching region of carbonyl groups. This band is red-shifted in comparison to the free carbonyl stretch of uracil, centred about 1750 cm^{-1} in the gas phase [60], presumably due to hydrogen bonding and carbonyls that are ligated to the metal cation which have the effect of lengthening and weakening the carbonyl bond. This band is even red-shifted in comparison with sodiated uracil, where the stretch is observed to be between 1630 and 1675 cm^{-1} [28]. The dicationic nature of the metal ions leads to further weakening of the metal coordinated C=O bond compared to sodium, results in a lower stretching frequency. Complexes of Ba^{2+}, Sr^{2+}, Ca^{2+} and Mg^{2+} each exhibit a second band centred between 1530–1548 cm^{-1} attributed to the enolic C-OH stretch expected in these dimers (*vide infra*). ~~This is again a red-shift of previous results, which found the enol C-OH stretch in protonated uracil to be centered about 1600 cm^{-1} [61].~~

Along with some weak features at lower energy, the $[M(Ura\text{-}H)(Ura)(H_2O)]^+$ spectra (Figure 1B) also contain two prominent carbonyl stretching bands. The most intense band is significantly blue-shifted by between 10 and 30 cm^{-1} compared to the same band for bare

$[M(Ura-H)(Ura)]^+$. The enol C-OH stretching bands are also blue-shifted by about 10–20 cm^{-1} upon hydration. These blue-shifts observed upon hydration are most likely the result of water binding to the metal and donation of electron density back to the remainder of the complex, particularly the carbonyl bonds; an inductive effect that results in a mild strengthening of the C=O bond.

Another interesting observation is that as the metal gets lighter over the Ba, Sr, and Ca series, the intense carbonyl stretching bands shift slightly from 1621 to 1617 to 1612 cm^{-1}, but for Mg, the band is observed at 1629 cm^{-1}. A similar pattern of shifting in position of that band for the hydrated complexes are observed although more pronounced—1648, 1637, 1625 cm^{-1} for the hydrated Ba, Sr, and Ca complexes, but 1645 cm^{-1} for the Mg complex. While the shifts for Ba, Sr, and Ca can be rationalized as being due to stronger metal-uracil binding for the smaller, more densely charged ions, we are unsure of why the band in the Mg complex are so much to the blue of the other C=O stretching bands.

3.2. Computed Structures for $[M(Ura-H)(Ura)]^+$. A total of 26 isomers were found for the Ba^{2+} and Ca^{2+} complexes, and 25 isomers were obtained for Sr^{2+} and Mg^{2+}. In Figure 2 the geometries and energetics for the three lowest energy structures are presented. In Figures S1 to S4, all structures and energies are presented for the Method 1 calculations and in Table S1, the energetics of five lowest energy structures are compared. The N3O4/N3O2(O4-O2) structures is lowest energy structure in the case of the Ba^{2+}, Sr^{2+} and Ca^{2+} complexes and is second by a negligible amount for Mg^{2+}. This is in agreement with previous results for Sr^{2+} and Ba^{2+} [31], and is consistent with results previously obtained for other dications, notably Pb^{2+} [22] and Cu^{2+} [27]. In this structure, one uracil is deprotonated at N3, with metal coordination to N3 and O4.

The neutral uracil is a tautomer where hydrogen has been transferred from N3 to O4, and the metal is coordinated to N3 and O2. Tetradentate interactions are confirmed by the Bader topological analysis, since four bond critical points (BCPs) connecting the metal to the two uracil units, are systematically found. Furthermore positive values of the Laplacian of the electron density $\nabla^2\rho$, indicates the electrostatic nature of these interactions (see Supporting Information). An intramolecular hydrogen bond is found between O4H of the neutral uracil and O2 of the deprotonated uracil, and is fairly strong, predicted to be only ~1.48 Å for all metals. This hydrogen bonding is confirmed by the topological analysis (low electron density, positive $\nabla^2\rho$). The enolic C-OH bond length is significantly longer, ~1.29 Å, than the other carbonyl bonds, all ~1.2 Å or less. The hydrogen bond established also induces a slight decrease in the electron density of the C2=O2 BCP. The weakening of the carbonyl groups interacting with the metallic centre is also evidenced by the topological analysis. Concerning the deprotonated uracil moiety, a decrease of 0.022-0.026 e a.u.$^{-3}$ of the electron density at the C4=O4 BCP is observed with respect to deprotonated uracil (dU, Supporting information). The effect is even more pronounced (0.034-0.040 e a.u.$^{-3}$) for the C2=O2 carbonyl group with the neutral U2 tautomer (the carbonyl denoted C2'=O2' in the SI for the sake of clarity). Furthermore, as would be expected, the two metal coordinated carbonyl bond lengths decrease slightly with increasing metal size due to decreasing metal-carbonyl bond strengths. The electron densities at the BCPs vary accordingly. This decrease in the electron density is also consistent with the red-shifts observed experimentally and described in the previous section (*vide supra*). The M-N and M-O bond lengths obviously increase as the metal cation size increases. Also, the M-N bond lengths and M-O bond lengths are between 0.11 and 0.21 Å and between 0.02 and 0.06 Å, respectively,

shorter for the deprotonated uracil compared to neutral uracil. All these trends are confirmed by the electron densities calculated at the corresponding BCPs.

These structural deviations away from the neutral, diketo tautomer as a result of the presence of the metal ion can have biological impacts through the disruption of hydrogen bonding between base pairs [62–64]. Both the deprotonation as well as the keto-enol proton transfer change the hydrogen bonding environment and may have a negative effect on the structural integrity of the nucleic acid strand, specifically RNA in the case of uracil.

Two additional structures in Figure 2 found to be slightly higher in energy are labelled as N3O4/N3O4(O2-O2) and N3O2/N3O2(O4-O4). In the N3O4/N3O4(O2-O2) structure, the metal is coordinated to the N3 and O4 of the uracil where the proton has been transferred to O2, and an intermolecular hydrogen bond is formed between O2H of uracil, and O2 of deprotonated uracil. This structure increases in computed relative energy compared to N3O4/N3O2(O4-O2) as the metal cation increases in size. The third structure, N3O2/N3O2(O4-O4) instead has metal coordination to N3 and O2 of both uracils, proton transfer from N3 to O4, and an intermolecular hydrogen bond between O4H and the O4 of deprotonated uracil. The N3O4/N3O4(O2-O2) isomer is slightly lower in energy when compared to N3O2/N3O2(O4-O4) when bound by a Sr^{2+} or Ca^{2+} ion. However, this order is reversed when Ba^{2+} is the metal center. For the complexes of Ba and Sr, these two isomers are within 1 kJ mol^{-1} of each other in terms of both enthalpy and Gibbs energy based upon the second calculation method. All other structures were determined to be significantly higher in energy by both methods of calculation by a minimum of about 15 kJ mol^{-1} in Gibbs energy.

All lowest energy structures are planar with method 1, but with method 2 the lowest energy Ba^{2+} and Sr^{2+} structures are slightly out of plane.

As a comparison the three lowest energy isomers for the $[Ca(Ura-H)(Ura)]^+$ complex were reoptimized, with def2-TZVPP basis set on all atoms. These results are also summarized in Table S1, and minimal deviation was noted between these and the results of method 2.

3.2.1. Comparison of Computed and Experimental Spectra. A comparison between the experimental spectra and the three lowest energy structures computed via method 2 are given in Figure 3 for the $[M(Ura-H)(Ura)]^+$ ions. The five lowest energy structures, based on both calculation methods, are compared to the experimental spectra for all ions in Figs. S5 to S12. For $[Ba(Ura-H)(Ura)]^+$ (Fig. 3A), there is good agreement between the experimental spectrum and those computed for structures i and iii. The major band of the experimental spectrum with a maximum at 1620 cm^{-1} is expected to be composed of four modes corresponding mainly to the stretching of the three C=O bonds and the C=C bonds. Complexes of Ba^{2+}, Sr^{2+}, Ca^{2+} and Mg^{2+} each exhibit a second less intense band centred between 1530–1548 cm^{-1} , which according to the comparison with calculations, can attributed to the enolic C4-O4H stretch expected in these dimers. In protonated uracil, the C4-O4 stretch was computed at 1487 cm^{-1} and could account for an experimental signal observed at 1469 cm^{-1} (REF CPC2007). Consequently, if we strictly compare the same bond, one observes a blue-shift with respect to protonated uracil. This blue-shift is in agreement with the AIM analysis, the electron density at the C4-O4 bond BCP for protonated uracil being 0.330 e $a.u.^{-3}$ while it ranges from 0.341 to 0.346 e $a.u.^{-3}$ for the N3O4/N3O2(O4-O2) structures. The C4-O4H bond is therefore reinforced in the complexes. This blue-shift is even more pronounced with respect to the neutral form of uracil involved in the complexes (tautomeric form U2).

There are no distinguishing features with which we can experimentally differentiate between these two lowest energy structures as was the case in 3200–3800 cm^{-1} region. It was not possible, in the 3200–3800 cm^{-1} region, to rule out the BaN3O4/N3O4(O2-O2) structure based on comparing the experimental and computed spectra [31]. However, based upon the poor agreement between the present experimental spectra and that computed for BaN3O4/N3O4(O2-O2) we can safely rule it out as being a major contributor, though its presence cannot be discounted entirely. Similar results are obtained for both the $[Sr(Ura-H)(Ura)]^+$ and $[Ca(Ura-H)(Ura)]^+$ complexes (Fig 3 B and C, respectively), although in both cases the N3O4/N3O4(O2-O2) isomer which does not have an apparent significant contribution is computed to be lower in energy than N3O2/N3O2(O4-O4).

For $[Mg(Ura-H)(Ura)]^+$, based on the computed spectra, we can safely rule out the second structure Mg-N3O4/N3O4(O2-O2) as the primary contributor even though it is computed to be the lowest energy structure, albeit only slightly. This may be due in part to the presence of a solvent effect which could be destabilizing the Mg-N3O4/N3O4(O2-O2) structure. As was the case for the other metals, neither the N3O4/N3O2(O4-O2) nor the N3O2/N3O2(O4-O4) structures can be ruled out by comparing the computed and experimental spectra, however, the latter is computed to be 9.3 kJ mol^{-1} higher in Gibbs energy. Due to time restrictions on the FEL we were not able to obtain the spectrum below 1400 cm^{-1} for the Mg complex, however, as for the other metals this region is not expected to differentiate between these isomers.

3.3. Computed Structures for $[M(Ura-H)(Ura)(H_2O)]^+$. The isomers that were examined computationally were all based upon the three lowest energy isomers of the unsolvated complexes. A total of 12 isomers were identified for the Ba^{2+} metal center, 13 isomers for Sr^{2+}, 9

isomers for Ca^{2+}, and 7 isomers for Mg^{2+}, for calculation Method 1 and can be seen in Figures S13-16. For $[Sr(Ura-H)(Ura)(H_2O)]^+$ using Method 2, only 11 isomers were obtained. The N3O4/N3O2(O4-O2)/wO4a isomer optimizes to N3O4/N3O2(O4-O2)/wO4b, while the N3O2/N3O2(O4-O4)/wO2a optimizes to N3O2/N3O2(O4-O4)/wO2b. A comparison of computed thermochemistries for both computational methods and the five lowest energy structures is given in Table S2.

As it was for the bare complexes, the lowest energy structure for the hydrated Ba^{2+}, Sr^{2+} and Ca^{2+} complexes share a common construction. The N3O4/N3O2(O4-O2) isomer which was determined to be the lowest energy configuration for the unsolvated complexes also forms the basis of these structures. The single water molecule is coordinated to the metal ion, and according to the Bader topological analysis (Supporting Information), also is participating in a hydrogen bond with O4 of the deprotonated uracil for Sr and Ba. Although a BCP is not localized for Ca, a weak interaction should be established as the water molecule is clearly oriented towards O4. This structure is identified as N3O4/N3O2(O4-O2)/wO4b, where 'O4b' is used to indicate hydrogen bonding between the water molecule and O4 of the deprotonated uracil (whereas the use of 'a' signifies a hydrogen bond involving the neutral uracil). The water molecule does not reside in the same plane as the remainder of the complex. The intramolecular hydrogen bond length between uracil molecules increased with increasing size of the metal center, from 1.477Å in the Mg^{2+} complex to 1.514Å in the Ba^{2+} complex. This is consistent the the decrease in the electron density at the corresponding BCP. An opposite trend is observed for the hydrogen bond between water and uracil, which ranges from 2.037 Å in Ba^{2+} to 2.424 Å in Ca^{2+}, and is virtually non-existent for Mg^{2+}, presumably due to the very strong Mg-OH_2 bond. Once again a slight increase in the enol C-OH bond length is expected with increasing metal

size, from 1.290 Å for Mg to 1.298 Å for Ba. This C-OH bond is clearly a single bond as confirmed by the computed ellipticity values. The single bond character is reinforced when increasing the size of the metal (decrease in ellipticities). There is no change in the length of the hydrogen bonded carbonyl bond, while the metal coordinated carbonyl bonds tend to increase in length with decreasing metal size, as was observed for the bare ions. Accordingly, the electron density at the BCP remains unchanged for this carbonyl group.

Similar to the unsolvated complexes, Mg^{2+} does not match the lowest energy structures of the other metals. As previously observed for the bare ion, the N3O4/N3O4(O2-O2) isomer is the lowest in energy when solvated, although in both cases, they are virtually isoenergetic. The water molecule is not planar with the remainder of the complex, however in all isomers where water is coordinated to Mg^{2+}, the water molecule does not participate in hydrogen bonding with the neighbouring uracils to the same extent as for the other metal complexes. Indeed, no BCP were found between water and the carbonyl groups of uracils.

Upon addition of a water molecule to the N3O4/N3O2(O4-O2) the structure around the metal cation relaxes somewhat. For all metals the M-N bonds increase by about 0.04 Å structures. The M-O bonds to the deprotonated and neutral uracils increase by between 0.05 and 0.09 Å and by between 0.02 and 0.03 Å, respectively. Consistently, on can see a decrease in the electron density at the BCPs with respect to bare complexes. This predicted loosening about the M-O and M-N bonds does not translate to a noticeable predicted decrease in the carbonyl bonds, and in some cases there are slight increases, but only in the thousandths of an angstrom. Experimentally, it is likely that a very small increase in the carbonyl bond strength could be responsible for the blue-shifting observed in the infrared spectra upon hydration, however, the calculations are not sensitive enough to reproduce this.

3.3.1. Comparison of Computed and Experimental Spectra. The experimental spectra for the $[M(Ura-H)(Ura)(H_2O)]^+$ ions are compared to the computed spectra for three of the lowest energy structures obtained computationally in Figure 5. The five lowest energy structures, based on both calculation methods, are compared to the experimental spectra for all ions in Figs. S17 to S24. In the case of Ba, Sr and Ca exceptional agreement is obtained between the experimental and calculated lowest energy spectra for the N3O4/N3O2(O4-O2)/wO4b tautomer. The intense band at 1648 cm^{-1} for the Ba^{2+} complex has an asymmetry about it which is most likely an unresolved shoulder at a slightly lower wavenumber position. The main band and the asymmetry are identified in the spectrum of the lowest energy complex as carbonyl stretches. Through calculations, the highest frequency stretch is expected to be the carbonyl participating in the intramolecular hydrogen bond with the enol, followed by the metal-coordinated carbonyl without water and then the metal-coordinated carbonyl hydrogen bonded to the water molecule, at scaled frequencies of 1662, 1637 and 1626 cm^{-1} respectively. The enol COH stretch at 1547 cm^{-1} is evident in the lowest energy spectrum at 1535 cm^{-1}. The N3O4/N3O4(O2-O2)/wO4b structures can all be ruled out as major contributors based on the disagreement with the computed and experimental spectra. However, as was the case for the bare ions, the N3O2/N3O2(O4-O4)/wO2b structure cannot be experimentally ruled out although they are higher energy structures. Similar experimental and computed spectra are observed for the Sr^{2+}, Ca^{2+}, and Mg^{2+} complexes. In figure S17 to S24, comparisons between some higher energy structures and the experimental spectra are made. There is not as good agreement between the computed and experimental spectra and based on the computed thermochemistry, it is not expected that these structures would be present in any observable quantity.

3.4 Comparison of Computational Methods. Thermodynamic data for the five lowest energy structures can be seen in Table S1 for $[M(Ura\text{-}H)(Ura)]^+$ complexes, and Table S2 for $[M(Ura\text{-}H)(Ura)(H_2O)]^+$ complexes. Both methods identify the same isomer as being the lowest in energy for each case. As well, good agreement is obtained in the trend of relative enthalpies and Gibbs energies for all other configurations. There is larger deviation in the relative energies of the two high energy bare complexes for Ba^{2+} and Sr^{2+} (ie. between the LANL2DZ and def2TZPP basis sets) but the relative energies for all the isomers for Ca^{2+} and Mg^{2+} are virtually identical (ie. 6-311+G(3df,3pd) and def2TZVPP).

A comparison of computed spectra are shown in Fig. S25. For $[Ba(Ura\text{-}H)(Ura)]^+$ and $[Ba(Ura\text{-}H)(Ura)(H_2O)]^+$ and shows that both spectra for each are remarkably similar. Either basis set (LANL2DZ or def2TZVPP) on the metal proves to be suitable for comparison with experimental data.

4. Summary

The structures of $[M(Ura\text{-}H)(Ura)]^+$ and $[M(Ura\text{-}H)(Ura)(H_2O)]^+$, where M corresponds to group 2 metal ions Ba^{2+}, Sr^{2+}, Ca^{2+} and Mg^{2+}, were examined using IRMPD spectroscopy in the mid-infrared 1000–1900 cm^{-1} region. Two different electronic structure calculation methods were used and compared to the experimental spectra and their energies were compared. There was good agreement between both computational methods in terms of the lowest energy structures and the IR spectra generated for these structures also correspond well to experimental IRMPD spectra. In the case of Mg^{2+} complexes, a second, virtually isoenergtic isomer, displays

better agreement with experimental spectra, and corresponds to the lowest-energy forms obtained with the three other metals.

In all cases, experimental evidence suggests the deprotonation of uracil occurs at the N3 position and that the neutral uracil is the tautomer where hydrogen is transferred from N3 to O4. This hydrogen then participates in a strong hydrogen bond interaction with O2 of the deprotonated uracil. The metal ion is tetracoordinate, interacting with N3 and O4 of the deprotonated uracil, and N3 and O2 of the other uracil, as confirmed by the AIM analysis. In the case of solvated structures, the complex takes an identical form, with the water molecule coordinated directly to the metal ion, and also hydrogen bonds with O4 of the deprotonated uracil. In the case of Mg^{2+} complexes, although these particular configurations are not calculated to be the lowest energy, it does provide the best agreement with the experimental IRMPD spectra and is only very slightly higher ($\leq$0.8 kJ·mol^{-1}) in energy.

Although for both the bare and solvated Mg^{2+} complexes two structures were computed to be very similar in energy, one could be ruled out as the primary structure based on spectroscopic evidence: The same one that could also be ruled out spectroscopically for the other metal ions. This second structure, that only differed slightly, could not be ruled out spectroscopically for Sr^{2+} and Ba^{2+} in a previous study focussed on the N-H stretching region.

Acknowledgements

The authors wish to thank the CLIO team (J. M. Ortega, C. Six, G. Perilhous, J. P. Berthet) as well as P. Maître and V. Steinmetz for their support during the experiments. The authors also acknowledge the computational resources provided by ACE-Net and Westgrid. Finally, TDF acknowledges the financial contributions from NSERC, CFI, and Memorial University.

Figure Captions

Scheme 1. Numbering scheme for uracil.

Figure 1. Comparison of IRMPD spectra for $[M(Ura-H)(Ura)]^+$ and $[M(Ura-H)(Ura)(H_2O)]^+$ complexes, M=Ba, Sr, Ca, Mg, in the 1000–1900 cm^{-1} region.

Figure 2. Comparison of the energies and structures for the three lowest energy $[M(Ura-H)(Ura)]^+$ complexes, M=Ba, Sr, Ca, Mg. The thermochemistry reported here are those from method 2.

Figure 3. Experimental IRMPD spectrum (bottom) for $[M(Ura-H)(Ura)]^+$ compared with the B3LYP computed spectra using computational method 2 for the three lowest energy structures. Lowest energy structures represent the (i) N3O4/N3O2(O4-O2), (ii) N3O4/N3O4(O2-O2) and (iii) N3O2/N3O2(O4-O4) tautomers. The calculated relative enthalpies and 298 K Gibbs energies (italics) are also shown.

Figure 4. Comparison of the energies and structures for the three lowest energy $[M(Ura-H)(Ura)(H_2O)]^+$ complexes, M=Ba, Sr, Ca, Mg. The thermochemistry reported here are those from method 2.

Figure 5. Experimental IRMPD spectrum (bottom) for $[M(Ura-H)(Ura)(H2O)]^+$ compared with the B3LYP computed spectra using computational method 2 for the three lowest energy

structures. Lowest energy structures represent the (i-w) N3O4/N3O2(O4-O2)/wO4b, (ii-w) N3O4/N3O4(O2-O2)/wO4b and (iii-w) N3O2/N3O2(O4-O4)/wO2b tautomers. The calculated relative enthalpies and Gibbs energies (italics) are also shown.

5. References

[1] A.M. Pyle, Science 261 (1993) 709.
[2] V.K. Misra, D.E. Draper, Biopolymers 48 (1998) 113.
[3] E. Madore, C. Florentz, R. Giege, J. Lapointe, J. Nucleic Acids Res. 27 (1999) 3583.
[4] R. Hanna, J.A. Doundna, Curr. Opin. Chem. Biol. 4 (2000) 166.
[5] D.L. Nelson, M.M. Cox, Lehninger, Principles of Biochemistry, 3rd ed., W.H. Freeman, New York, 2004, Chapter 10.
[6] G.L. Eichhorn, L.G. Marzilli, Advances in Inorganic Biochemistry: Metal Ions in Genetic Information Transfer, vol. 3, Elsevier Science, New York, 1981, p.1
[7] G.C. Eichhorn, Nature 194 (1962) 474.
[8] W. Förster, E. Bauer, H. Schutz, H. Berg, M. Akimenko, L.-E. Minchenkova, Y.M. Evdkimov, Y.M. Vershavsky, Biopolymers 18 (1979) 625.
[9] A.M. Pyle, J. Biol. Inorg. Chem. 7 (2002) 679.
[10] S. Basu, R.P. Rambo, J. Strauss-Soukup, J.H. Cate, A.R. Ferre-D'Amare, S.A. Strobel, J.A. Doudna, Nat. Struct. Biol. 5 (1998) 986.
[11] R. Shiman, D.E. Draper, J. Mol. Biol. 302 (2000) 79.
[12] Y.A. Shin, G.L. Eichhorn, Biopolymer 16 (1977) 225.
[13] S. Burge, G.N. Parkinson, P. Hazel, A.K. Todd, S. Neidle, Nucleic Acids Res. 34 (2006) 5402.
[14] P.-O. Lowdin, Rev. Mod. Phys. 35 (1963) 724.
[15] M.D. Topal, J.R. Fresco, Nature 263 (1976) 285.
[16] P.O.P. Ts'o, Basic Principles in Nucleic Acids Chemistry, Academic, New York, 1974.
[17] H. Ruterjans, E. Kaun, W.E. Hull, H.H. Limbach, Nucleic Acid Res. 10 (1982) 7.
[18] S. Guillaumont, J. Tortajada, J.-Y. Salpin, A. M. Lamsabhi, Int. J. Mass Spectrom. 243 (2005) 279.
[19] C. Gutlé, J.-Y. Salpin, T. Cartailler, J. Tortajada, M.-P. Gaigeot, J. Phys. Chem. A 110 (2006) 11684.
[20] M. Kabeláč, P. Hobza, J. Phys. Chem. B 110 (2006) 14515.
[21] J.-Y. Salpin, S. Gauilloumont, J. Tortajada, A. Lamsabhi, J. Am. Soc. Mass Spectrom. 20 (2009) 359.
[22] O.Y. Ali, T.D. Fridgen, Int. J. Mass Spectrom. 308 (2011) 167.
[23] E.A.L. Gillis, K. Rajabi, T.D. Fridgen, J. Phys. Chem. A 113 (2009) 824.
[24] E.A.L. Gillis, T. D. Fridgen, Int. J. Mass Spectrom. 297 (2010) 2.
[25] E. Rincón, M. Yáñez, A. Toro-Labbé, O. Mó, Phys. Chem. Chem. Phys. 9 (2007) 2531.
[26] A. Lamsabhi, M. Alcami, O. Mó, M. Yáñez, J. Tortajada, J. Phys. Chem. A 110 (2006) 1943.
[27] O.Y. Ali, T.D. Fridgen, ChemPhysChem 13 (2012) 588.
[28] Y.-w. Nei, T.E. Akinyemi, C.M. Kaczan, J.D. Steill, G. Berden, J. Oomens, M.T. Rodgers, Int. J. Mass Spectrom 308 (2011) 191.
[29] J.-Y. Salpin, S. Guillaumont, D. Ortiz, J. Tortajada, P. Maître, Inorg. Chem. 50 (2011) 7769.
[30] O.Y. Ali, N.M. Randell, T.D. Fridgen, ChemPhysChem 13 (2012) 1507.
[31] A.A. Power, O.Y. Ali, M.B. Burt, T.D. Fridgen, Int J of Mass Spectrom, 330–332 (2012) 233.
[32] A. Eizaguirre, A.M. Lamsabhi, O. Mo, M. Yanez, Theor. Chem. Acc., 128 (2011) 457.

[33] D. Dougherty, K. Wittel, J. Meeks, S.P. McGlynn, J. Am. Chem. Soc. 98 (1976) 3815.
[34] R. Czerminski, B. Lesying, A. Pohorille, Int. J. Quantum Chem. 16 (1979) 605.
[35] D. Shugar, K. Szczepaniak, Int. J. Quantum Chem. 20 (1981) 573.
[36] P. Beak, J.M. White, J. Am. Chem. Soc. 104 (1982) 7073.
[37] M. Szczesniak, M.J. Nowak, K. Szczepaniak, W.B. Person, D. Shugar, J. Am. Chem. Soc. 105 (1983) 5969.
[38] S. Chin, I. Scott, K. Szczepani, W.B. Person, J. Am. Chem. Soc. 106 (1984) 3415.
[39] M.J. Scanlan, I.H. Hillier, J. Am. Chem. Soc. 106 (1984) 3737.
[40] J.S. Kwiatkowski, T.J. Zielinski, R. Rein, Adv. Quantum Chem. 18 (1986) 85.
[41] U. Norinder, THEOCHEM 36 (1987) 259.
[42] Y. Tsuchiya, M. Fujii, M. Ito, J. Phys. Chem. 92 (1988) 1760.
[43] B.B. Brady, L.A. Peteanu, D.H. Levy, Chem. Phys. Lett. 147 (1988) 538.
[44] R.D. Brown, P.D. Godfrey, D. McNaughton, A.P. Pierlot, J. Am. Chem. Soc. 110 (1988) 2329.
[45] A. Leś, L. Adamowicz, J. Phys. Chem. 93 (1989) 7078.
[46] I.R. Gould, I.H. Hiller, J. Chem. Soc. Perkin Trans. 2 (1990) 329.
[47] J. Leszczynski, J. Phys. Chem. 96 (1992) 1649.
[48] D.A. Estrin, L. Paglieri, G. Corongiu, J. Phys. Chem. 98 (1994) 5653.
[49] I.R. Gould, N.A. Burton, R.J. Hall, I.H. Hiller, THEOCHEM 331 (1995) 147.
[50] L. Paglieri, G. Corongiu, D.A. Estrin, Int. J. Quantum Chem. 56 (1995) 615.
[51] S.X. Tian, C.F. Zhang, Z.J. Zhang, X.J. Chen, K.Z. Xu, Chem. Phys. 242 (1999) 217.
[52] M. Sabat, B. Lippert, Met. Ions Biol. Syst. 33 (1996) 143.
[53] C. Trujillo, A.M. Lamsabhi, O. Mó, M. Yáñez, J.-Y. Salpin, Org. Biomol. Chem., 6 (2008) 3695.
[54] R. Prazeres, F. Glotin, C. Insa, D. A. Jaroszynski, J. M. Ortega, Eur. Phys. J. D, 3 (1998) 87.
[55] W. Paul, Rev. Mod. Phys., 62 (1990) 531.
[56] K. Rajabi, M. L. Easterling, T. D. Fridgen, J. Am. Soc. Mass Spectrom., 20 (2009) 411.
[57] Gaussian 09, Revision D.01, M.J. Frisch, G.W. Trucks, H.B. Schlegel, G.E. Scuseria, M.A. Robb, J.R. Cheeseman, G. Scalmani, V. Barone, B. Mennucci, G.A. Petersson, H. Nakatsuji, M. Caricato, X. Li, H.P. Hratchian, A.F. Izmaylov, J. Bloino, G. Zheng, J.L. Sonnenberg, M. Hada, M. Ehara, K. Toyota, R. Fukuda, J. Hasegawa, M. Ishida, T. Nakajima, Y. Honda, O. Kitao, H. Nakai, T. Vreven, J.A. Montgomery, Jr., J.E. Peralta, F. Ogliaro, M. Bearpark, J.J. Heyd, E. Brothers, K.N. Kudin, V.N. Staroverov, T. Keith, R. Kobayashi, J. Normand, K. Raghavachari, A. Rendell, J.C. Burant, S.S. Iyengar, J. Tomasi, M. Cossi, N. Rega, J.M. Millam, M. Klene, J.E. Knox, J.B. Cross, V. Bakken, C. Adamo, J. Jaramillo, R. Gomperts, R.E. Stratmann, O. Yazyev, A.J. Austin, R. Cammi, C. Pomelli, J.W. Ochterski, R.L. Martin, K. Morokuma, V.G. Zakrzewski, G.A. Voth, P. Salvador, J.J. Dannenberg, S. Dapprich, A.D. Daniels, O. Farkas, J.B. Foresman, J.V. Ortiz, J. Cioslowski, D.J. Fox, Gaussian, Inc., Wallingford CT, (2013).
[58] P.B. Armentrout, M. Citir, Y. Chen, M.T. Rodgers, J. Phys. Chem. A, 116 (2012) 11823.
[59] P.B. Armentrout, Y. Chen, M.T. Rodgers, J. Phys. Chem. A, 116 (2012) 3989.
[60] P. Colarusso, K. Zhang, B. Gup, P.F. Bernath, Chem Phys Lett, 269 (1997) 39.
[61] J.-Y. Salpin, S. Guillaumont, J. Tortajada, L. MacAleese, J. Lemaire, P. Maître, ChemPhysChem, 8 (2007) 2235.

[62] S.J. Lippard, J.M. Berg, Principles of Bioinorganic Chemistry, University Science Books, Mill Valley CA, 1994.
[63] W. Kaim, B. Schwedersky, Bioinorganic Chemistry: Inorganic Elements in the Chemistry of Life, John Wiley & Sons, Chichester, 1994.
[64] L.A. Loeb, A.R. Zakour, In Nucleic Acids-Metal Ion Interactions, Spiro, T. G., Ed., John Wiley & Sons, New York, 1980, p. 115-144.

Scheme 1.

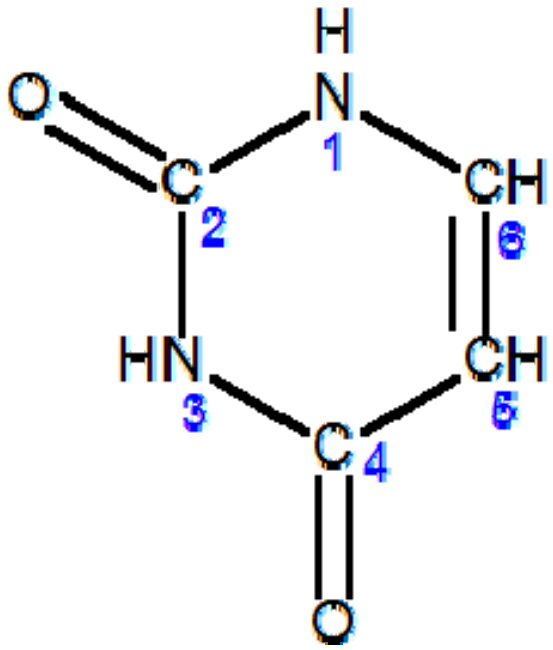

Figure 1.

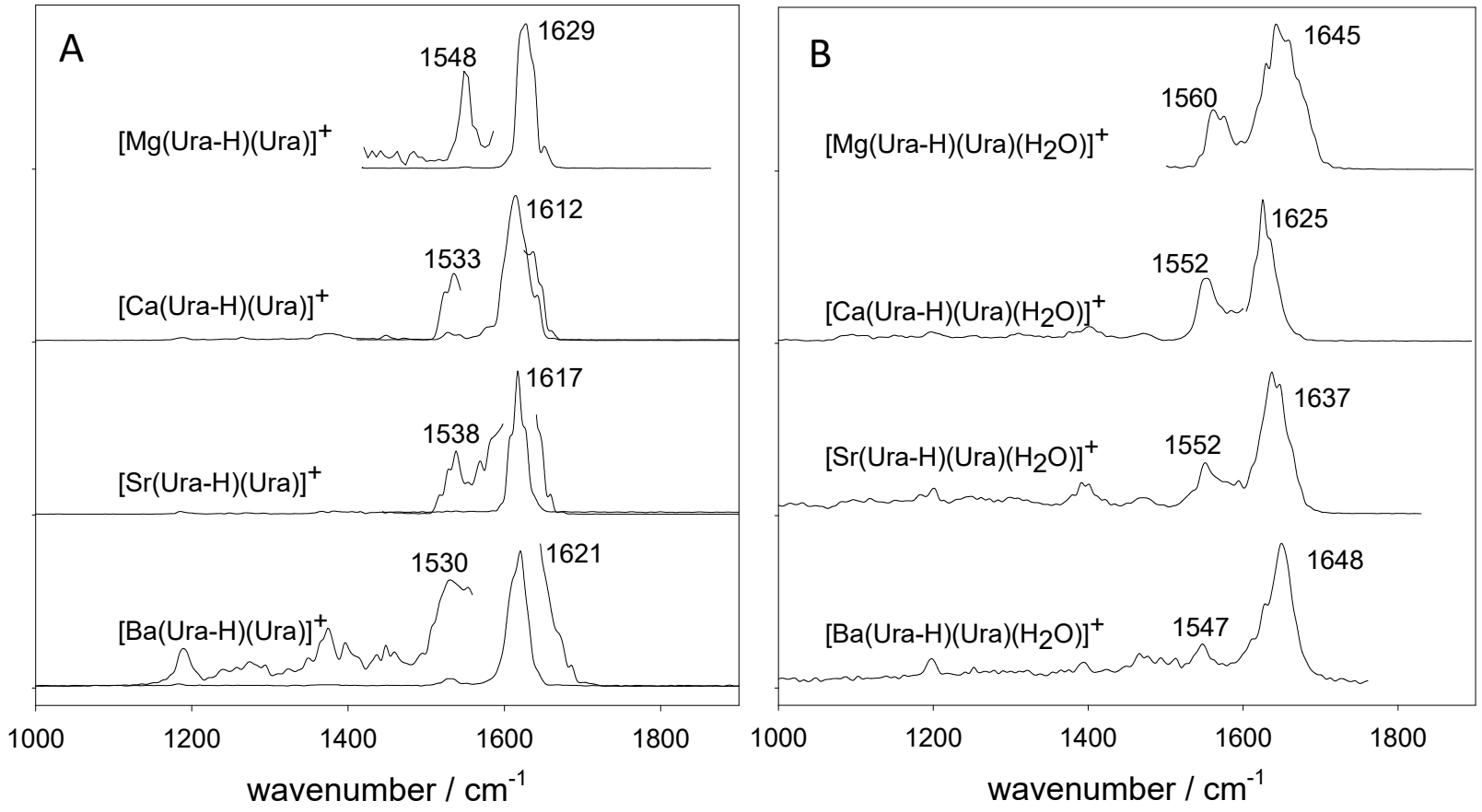
A
1548
1629
[Mg(Ura-H)(Ura)]+
1533
1612
[Ca(Ura-H)(Ura)]+
1538
1617
[Sr(Ura-H)(Ura)]+
1530
1621
[Ba(Ura-H)(Ura)]+
1000
1200
1400
1600
1800
wavenumber / cm-1
B
1560
1645
[Mg(Ura-H)(Ura)(H2O)]+
1552
1625
[Ca(Ura-H)(Ura)(H2O)]+
1552
1637
[Sr(Ura-H)(Ura)(H2O)]+
1547
1648
[Ba(Ura-H)(Ura)(H2O)]+
1000
1200
1400
1600
1800
wavenumber / cm-1

Figure 2.

iii

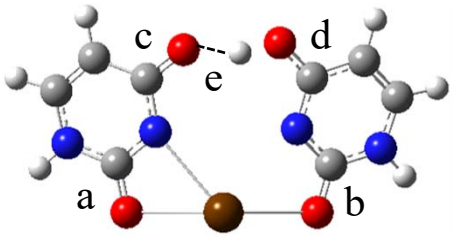

M-N3O2/N3O2(O4-O4)

M	$\Delta_{rel}H/\Delta_{rel}G$	a	b	c	d	e
Ba	4.1/4.1	1.270	1.260	1.255	1.291	1.444
Sr	4.1/4.1	1.272	1.262	1.254	1.287	1.424
Ca	4.7/5.3	1.275	1.266	1.254	1.285	1.412
Mg	9.3/9.1	1.279	1.272	1.253	1.283	1.420

ii

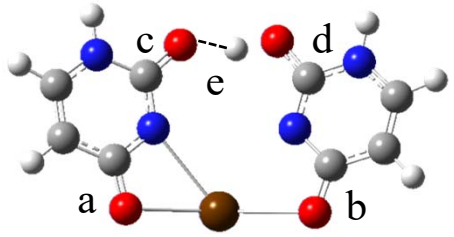

M-N3O4/N3O4(O2-O2)

M	$\Delta_{rel}H/\Delta_{rel}G$	a	b	c	d	e
Ba	4.7/4.8	1.272	1.263	1.258	1.291	1.406
Sr	3.8/3.9	1.273	1.264	1.257	1.288	1.392
Ca	2.6/2.3	1.276	1.268	1.256	1.285	1.380
Mg	0/0	1.281	1.274	1.255	1.283	1.388

i

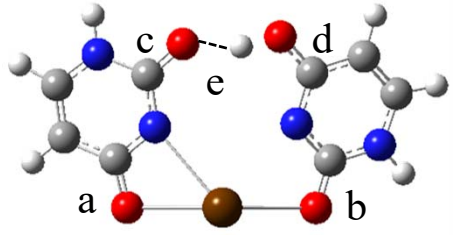

M-N3O4/N3O2(O4-O2)

M	$\Delta_{rel}H/\Delta_{rel}G$	a	b	c	d	e
Ba	0/0	1.274	1.259	1.252	1.295	1.493
Sr	0/0	1.276	1.261	1.251	1.292	1.478
Ca	0/0	1.279	1.264	1.250	1.290	1.473
Mg	0.8/0.6	1.283	1.270	1.248	1.288	1.487

Figure 3.

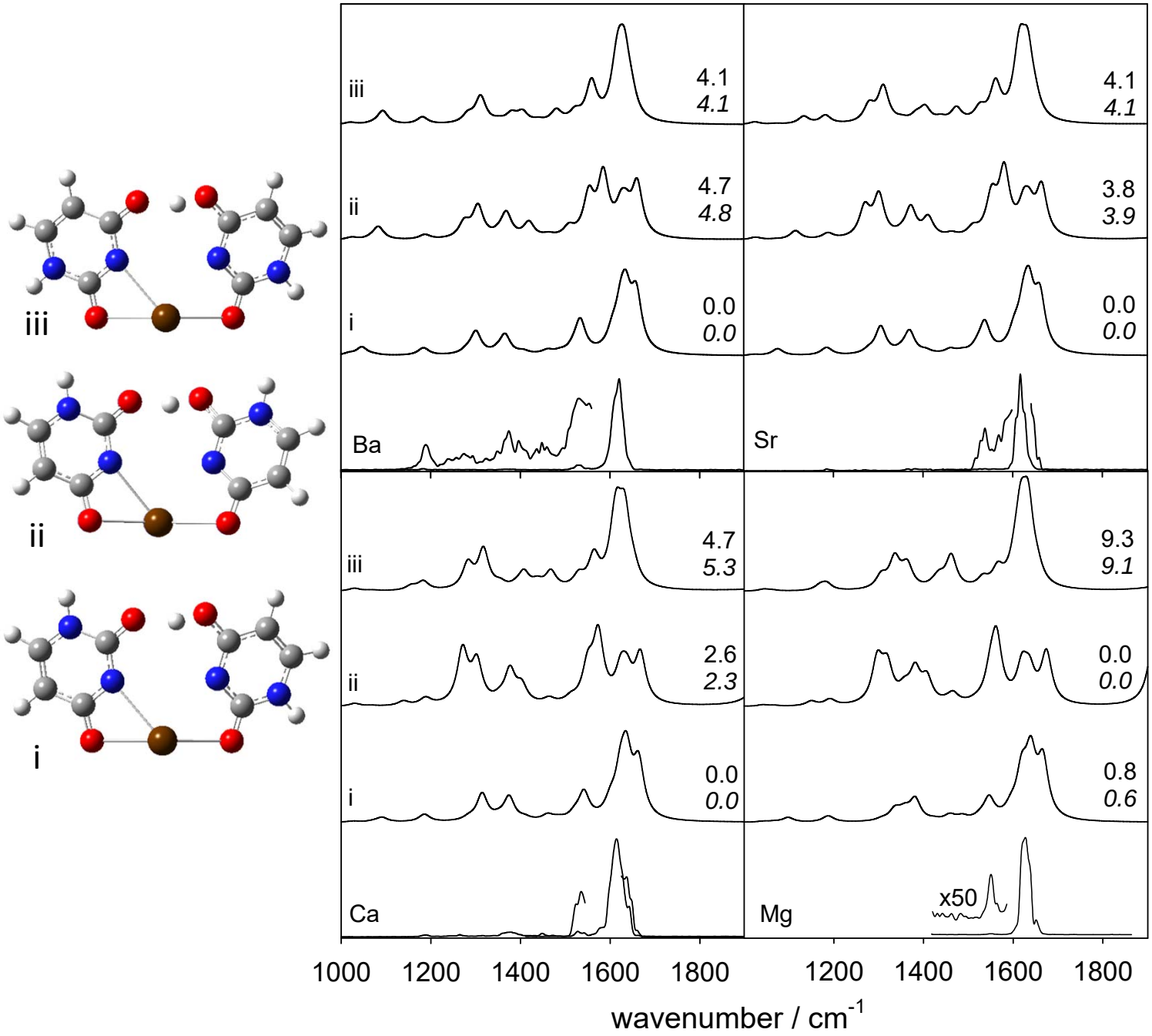
iii
ii
i
iii
4.1
4.1
ii
4.7
4.8
i
0.0
0.0
Ba
Sr
4.1
4.1
3.8
3.9
0.0
0.0
iii
4.7
5.3
ii
2.6
2.3
i
0.0
0.0
Ca
Mg
9.3
9.1
0.0
0.0
0.8
0.6
x50
1000
1200
1400
1600
1800
1200
1400
1600
1800
wavenumber / cm-1

Figure 4.

iii-w

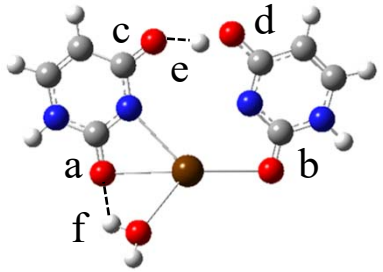

M-N3O2/N3O2(O4-O4)/wO2b

M	$\Delta_{rel}H/\Delta_{rel}G$	a	b	c	d	e	f
Ba	6.3/5.3	1.271	1.258	1.253	1.293	1.471	2.047
Sr	5.9/5.8	1.272	1.260	1.253	1.290	1.444	2.223
Ca	5.7/4.6	1.273	1.262	1.254	1.287	1.421	2.595
Mg	8.2/8.1	1.273	1.267	1.255	1.285	1.421	3.407

ii-w

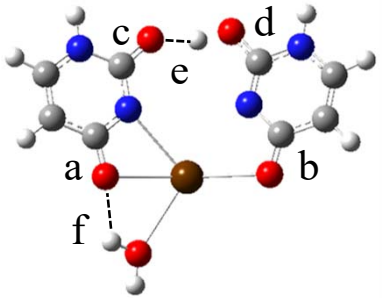

M-N3O4/N3O4(O2-O2)/wO4b

M	$\Delta_{rel}H/\Delta_{rel}G$	a	b	c	d	e	f
Ba	6.3/5.9	1.273	1.261	1.255	1.294	1.437	2.065
Sr	5.1/4.7	1.274	1.262	1.255	1.291	1.414	2.199
Ca	3.4/2.7	1.275	1.265	1.256	1.288	1.392	2.516
Mg	0/0	1.276	1.269	1.257	1.284	1.378	2.938

i-w

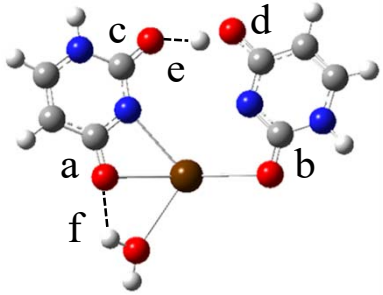

M-N3O4/N3O2(O4-O2)/wO4b

M	$\Delta_{rel}H/\Delta_{rel}G$	a	b	c	d	e	f
Ba	0/0	1.275	1.257	1.250	1.298	1.514	2.037
Sr	0/0	1.277	1.259	1.250	1.294	1.492	2.164
Ca	0/0	1.278	1.261	1.250	1.292	1.479	2.424
Mg	0.4/0.2	1.279	1.264	1.250	1.290	1.477	2.813

Figure 5.

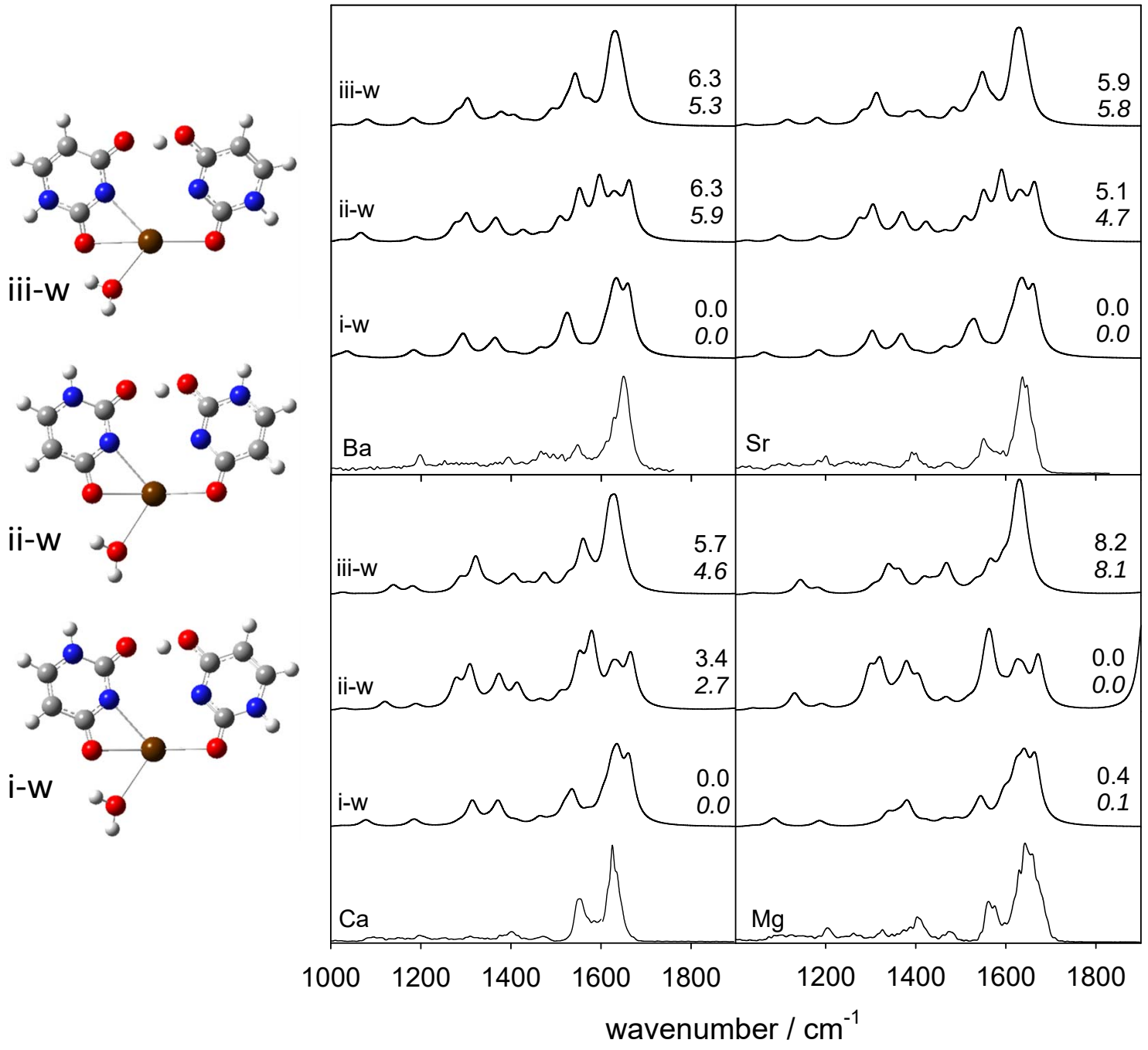
iii-w
ii-w
i-w
iii-w
6.3
5.3
ii-w
6.3
5.9
i-w
0.0
0.0
Ba
iii-w
5.7
4.6
ii-w
3.4
2.7
i-w
0.0
0.0
Ca
iii-w
5.9
5.8
ii-w
5.1
4.7
i-w
0.0
0.0
Sr
iii-w
8.2
8.1
ii-w
0.0
0.0
i-w
0.4
0.1
Mg
1000
1200
1400
1600
1800
1200
1400
1600
1800
wavenumber / cm-1